Ferromagnetism in chemically synthesized CeO_2 nanoparticles by Ni doping

A. Thurber,[1] K. M. Reddy,[1] V. Shutthanandan,[2] M. H. Engelhard,[2] C. Wang,[2] J. Hays,[1] and A. Punnoose[1,*]
[1]*Department of Physics, Boise State University, Boise, Idaho 83725-1570, USA*
[2]*Environmental Molecular Sciences Laboratory, Pacific Northwest National Laboratory, Richland, Washington 99352, USA*
(Received 21 July 2006; revised manuscript received 1 September 2007; published 24 October 2007)

This work reports the discovery of room-temperature ferromagnetism in 5–9 nm sized $Ce_{1-x}Ni_xO_2$ nanoparticles ($0.01 \leqslant x \leqslant 0.20$) prepared using a sol-gel based chemical method at room temperature and under ambient conditions. Particle induced x-ray emission studies were used to determine the dopant concentrations. Magnetic measurements of the chemically synthesized $Ce_{1-x}Ni_xO_2$ samples at room temperature showed coercivity in the 40–120 Oe range, and the saturation magnetization showed a maximum of 1.21 memu/g (8.59×10^{-4} μ_B/Ni ion) for $x=0.04$. Average crystallite sizes and lattice parameters estimated from x-ray diffraction and transmission electron microscopy studies showed a gradual decrease with x in the entire doping range, while the lattice strain showed a minimum for $x=0.04$. Optical studies revealed direct band gap energies ranging from 3.23 to 3.99 eV with a minimum for $x=0.04$. A high Curie temperature of $T_C=665$ K was obtained for $x=0.03$.

DOI: 10.1103/PhysRevB.76.165206 PACS number(s): 75.50.Pp, 81.16.Be

I. INTRODUCTION

Metal oxides have recently been the subject of intense research for applications in the spintronics field since the discovery of room-temperature ferromagnetism (RTFM) in dilute magnetic semiconductor oxide systems.[1–7] Tailoring the physical properties and adding new functionality to the existing materials by engineering the structure, composition, and particle and/or grain size are among the new approaches in advancing the current applications of materials. Preparing these materials in the nanoscale size range is more interesting due to the increased surface-to-volume ratio, which might affect the structural and most other physical properties. Transition-metal (TM) doping has been proposed to introduce magnetic functionality in conventional semiconductors and metal oxides.[1,2] Recent reports on the observation of RTFM in thin films and powders of TM-doped oxide semiconductors such as TiO_2,[3] ZnO,[3–5] and SnO_2 (Refs. 6 and 7) generated tremendous interest in investigating other metal oxide materials as well.

CeO_2, a robust rare earth oxide insulator, is a key material for a wide variety of applications such as a buffer layer for silicon on insulator devices,[8] a basis in field effect transistors,[9] and as a high-k dielectric material in capacitors.[10–12] These applications make CeO_2, already used in catalysis, electrolysis, and optical coatings,[13–18] a very interesting candidate to develop RTFM for use in novel multifunctional devices. It has recently been demonstrated that the wet chemical sol-gel process can be used to produce TM-doped metal oxides in the nanoparticle form with ferromagnetic (FM) properties.[6,19–21] Use of the sol-gel process to produce these materials in aerobic and ambient conditions aids in the intrinsic elimination of the formation of metallic particles, as opposed to other fabrication techniques.[22,23] When prepared as particles with sizes <50 nm, CeO_2 has recently been shown to display interesting nanoscale size effects on its physical properties.[24–26] Because of these reasons, we prepared Ni doped CeO_2 nanoparticles in the 5–9 nm size range. Our work reports the observation of ferromagnetism along with strong correlations between the magnetic, structural, and optical properties of CeO_2 nanoparticles as a result of Ni doping in the 0%–20% range. While metallic Ni particle formation is eliminated intrinsically due to the process employed, all the simple oxides of Ni as well as Ni-Ce-O binary and/or ternary systems are not FM, and there is no evidence from any of our studies suggesting the formation of any impurity phases within the samples. Tiwari *et al.*[27] have reported ferromagnetism in CeO_2 thin films grown on $LaAlO_3$ (001) substrates using pulsed laser deposition through Co doping, showing a giant magnetic moment of 6.1 μ_B/Co ion and a Curie temperature $T_C=875$ K for 3% Co doping. No such giant magnetic moments were observed in our $Ce_{1-x}Ni_xO_2$ samples; however, the magnetic, structural, and optical properties and the Curie temperatures of our samples depend strongly on the dopant concentration.

II. EXPERIMENTAL DETAILS

All $Ce_{1-x}Ni_xO_2$ samples were prepared in air at room temperature by adding $Ce(NO_3)_3 \cdot 6H_2O$ and $Ni(NO_3)_2 \cdot 6H_2O$ to de-ionized water to obtain a 0.01M solution with a molar ratio of $x=[Ni]/([Ni]+[Ce])$, to which a 4M NH_4OH solution was added until the pH level reached 9. The mixture was stirred for 2 h at room temperature and subsequently filtered, after which it was dried for 12 h at 50 °C. Annealing took place in air at 450 °C for 3 h in a tube furnace to produce the metal oxide nanoparticles. Differing amounts of $Ce(NO_3)_3 \cdot 6H_2O$ and $Ni(NO_3)_2 \cdot 6H_2O$ were used with target ratios meant to obtain a systematic variation of x in the 0%–20% range. The pure CeO_2 sample ($x=0$) was produced without adding any $Ni(NO_3)_2 \cdot 6H_2O$ for use as a reference. Similarly, a pure nickel oxide sample ($x=1$) prepared under identical conditions but without any $Ce(NO_3)_3 \cdot 6H_2O$ for comparison to the doped samples was found to be antiferromagnetic NiO. A physical mixture to obtain $[Ni]/([Ni]+[Ce])=0.05$, comparable to $Ce_{0.95}Ni_{0.05}O_2$, was also prepared using the samples of pure CeO_2 and NiO for compari-

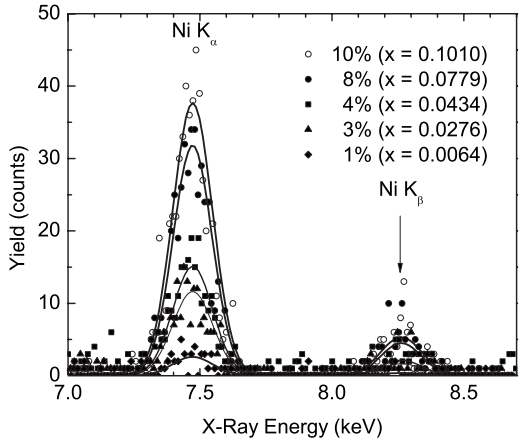

FIG. 1. PIXE data taken on $Ce_{1-x}Ni_xO_2$ samples showing actual Ni concentrations.

son to the doped samples, accomplished by grinding measured amounts of the pure samples together in an agate mortar.

Particle induced x-ray emission (PIXE) studies were conducted at the accelerator facility at the Pacific Northwest National Laboratory to determine the actual dopant concentrations.[19] Samples were irradiated with a 2.0 MeV He^+ ion beam, and the x rays emitted during the deexcitation process were analyzed with an x-ray spectrometer. Resulting PIXE spectra after removing the background due to Bremsstrahlung are shown in Fig. 1, giving Ni concentrations of 0.64%, 2.76%, 4.34%, 7.79%, and 10.10% [% given as molar ratio of [Ni]/([Ni]+[Ce]) estimated from atomic percentages]. Detailed characterization of samples was carried out using x-ray diffraction (XRD), spectrophotometry, magnetometry, x-ray photoelectron spectroscopy (XPS), electron diffraction (EDP), and high-resolution transmission electron microscopy (HRTEM). XRD patterns were recorded at room temperature using a Phillips X'Pert x-ray diffractometer in Bragg-Brentano geometry with a Cu $K\alpha$ source ($\lambda = 1.5406$ Å). Powder samples were leveled in the sample holder and placed on a horizontal mount. Diffuse reflectance data were recorded at room temperature using a Cary 5000 spectrophotometer by loading small amounts of powder samples into a horizontal sample holder and placing it inside the spectrophotometer. Transmission electron microscopy (TEM) and EDP experiments were done at the Pacific Northwest National Laboratory on a JEOL JEM 2010 microscope with a specified point-to-point resolution of 0.194 nm. The operating voltage of the microscope was 200 kV. All images were digitally recorded with a slow scan charge coupled device camera (image size of 1024×1024 pixels), and image processing was carried out using the DIGITAL MICROGRAPH software from Gatan (Pleasant, CA, USA). XPS measurements were performed using a Physical Electronics Quantum 2000 Scanning ESCA microprobe. This system uses a focused monochromatic Al $K\alpha$ x-ray (1486.7 eV) source and a spherical section analyzer. The x-ray beam used was a 100 W, 200 μm diameter spot rastered over a 1.4×0.2 mm^2 area on the sample. The x-ray beam was incident normal to the sample, and the photoelectron detector was at

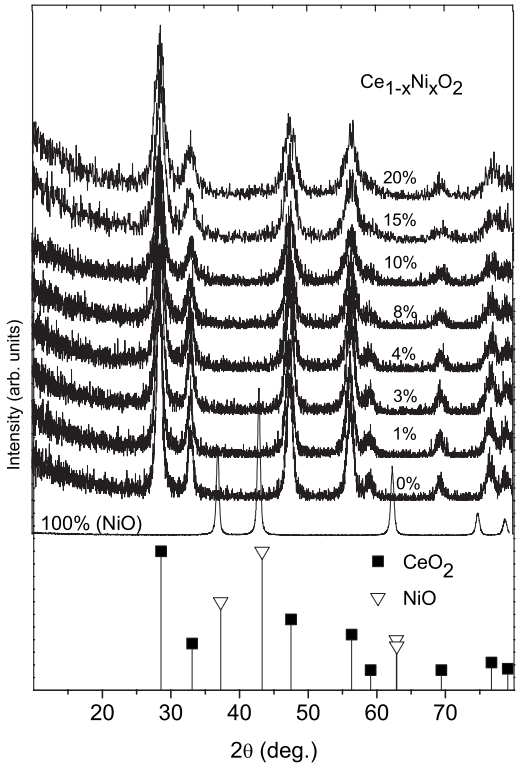

FIG. 2. XRD patterns recorded at room temperature for samples prepared at 450 °C with varying dopant concentration, including a pure NiO sample. Expected peak positions and intensities are shown for CeO_2 and NiO along the x axis.

45° off normal. The binding energy scale is calibrated using the Cu $2p_{3/2}$ feature at 932.62 ± 0.05 eV and Au $4f$ feature at 83.96 ± 0.05 eV for known standards. The samples experienced variable degrees of charging. Low energy electrons at ~1 eV, 20 μA and low energy Ar^+ ions were used to minimize this charging. Magnetic data were recorded using a LakeShore model 7404 vibrating sample magnetometer (VSM), which is also equipped with a high temperature oven. For the room-temperature VSM data, powder samples were tightly packed into a clear straw and mounted using a fiberglass rod. T_C measurements were done by loading the powder into a boron nitrite cup attached to the end of a quartz rod mounted inside the VSM oven.

III. RESULTS AND DISCUSSION

A. X-ray diffraction studies

The effects of Ni doping on the particle size and lattice structure of CeO_2 were investigated using XRD and TEM. The x-ray diffraction patterns obtained from all the $Ce_{1-x}Ni_xO_2$ samples with $x = 0-0.20$, shown in Fig. 2, showed strong cubic CeO_2 peaks. The XRD pattern of the Ni-only sample synthesized under identical conditions as the doped samples, but without using any cerium precursor ($x = 1$), also in Fig. 2, showed only cubic NiO, suggesting that any unincorporated Ni, if present in the sample, will form the antiferromagnetic NiO phase. The complete absence of even

the strongest peaks of nickel oxide in any of the doped samples indicates that no detectable amount of nickel oxide was produced in the sol-gel process employed to synthesize the $Ce_{1-x}Ni_xO_2$. All peaks in the doped $Ce_{1-x}Ni_xO_2$ samples ($x \leqslant 0.20$) are accounted for with the expected cubic CeO_2 reference lines. Peak positions and widths were determined by fitting the experimental data with a modified Lorentzian function given by

$$I = B + B_s x + \frac{I_0 W_h^2}{W_h^2 + (x - P)^2},$$

where B and B_s define the baseline, I_0 is the peak intensity in counts, W_h is the half-width at half maximum, and P is the peak position in $2\theta^\circ$. Peak position of the (111) plane was used to estimate the lattice parameter a of the cubic system as a function of x, and the observed variation is shown in Fig. 3(a). The full widths at half maximum of the peaks determined from this function were taken to be the measured width β_m. The instrumental width β_s was calculated using data taken on the same XRD diffractometer of a pure silica standard. The measured widths β_m were compared to the widths β_s of the nearest peaks from the silica sample to determine the true width β by the equation $\beta^2 = \beta_m^2 - \beta_s^2$. Once β was known, a plot of $\beta \cos\theta$ vs $\sin\theta$ was constructed and the data were fitted with a linear function. The lattice strain η and particle size D were estimated using the Scherrer relation:[24,28]

$$\beta \cos\theta = \frac{0.89\lambda_0}{D} + \eta \sin\theta,$$

where $\lambda_0 = 1.5406$ Å is the wavelength for the Cu $K\alpha$ radiation. The estimated average particle size D and lattice strain η are shown in Figs. 3(b) and 3(c), respectively. The average particle size D decreases from ~9 nm in pure CeO_2 to ~5 nm in the sample with $x = 0.10$, as shown in Fig. 3(b). For higher doping concentration up to $x = 0.20$, the particle size decreases further to ~4.5 nm. This indicates that Ni incorporation hinders crystallite growth as observed in other TM-doped metal oxide systems.[6,21] The pure NiO nanoparticles prepared under identical conditions, but without any Ce precursor, were estimated from XRD to be ~20 nm, much larger than the Ni doped CeO_2. In recent studies,[24–26] it has been shown that for CeO_2 nanoparticles, the lattice parameter increases dramatically with decreasing particle size. Based on experimental data and first-principles calculations, this rapid lattice expansion in the low (<10 nm) particle size regime resulted from an increasing concentration of Ce^{3+} ions replacing Ce^{4+} as well as an increasing number of oxygen vacancies. However, in our $Ce_{1-x}Ni_xO_2$ samples, the particle size is decreasing with increasing x in this same regime while the lattice parameter is decreasing. We attribute this opposite effect to the large difference between Ni and Ce ionic radii. The sizes of both Ce^{3+} and Ce^{4+} ions in all known coordinations are close to twice the ionic size of Ni^{2+}, Ni^{3+}, or Ni^{4+} ions irrespective of their coordination numbers.[29] Thus, the contraction of the lattice due to Ni ion incorporation overwhelms the reported nanoscale expansion effect. The undoped CeO_2 nanoparticles are under significant lattice

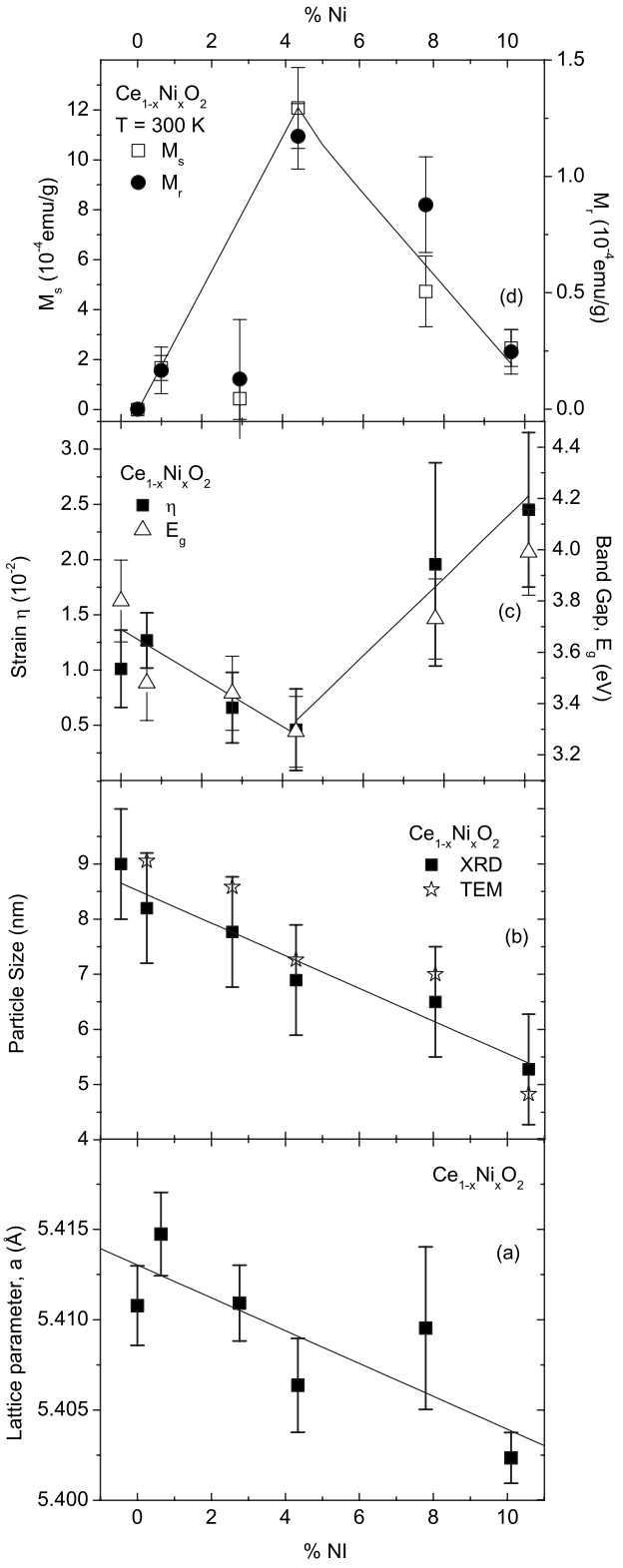

FIG. 3. (a) Lattice parameter for cubic CeO_2, (b) particle size from XRD and TEM, (c) strain estimated from analysis of XRD patterns and band gap energies E_g from diffuse reflectance, and (d) saturation magnetization M_s and remanent magnetization M_r all given as a function of x for the $Ce_{1-x}Ni_xO_2$ samples. Lines shown are linear fits of data for visual aid.

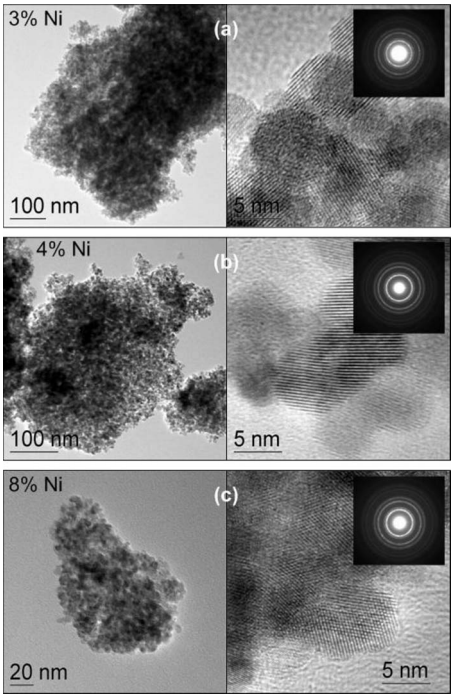

FIG. 4. HRTEM images and corresponding EDP data of $Ce_{1-x}Ni_xO_2$ samples for (a) $x=0.03$, (b) $x=0.04$, and (c) $x=0.08$.

strain [Fig. 3(c)], in agreement with recent reports on nanoscale cerium oxide with similar particle size,[30] and the positive sign indicates that the lattice has undergone an expansion. Such increased lattice strain observed in small nanoparticles of CeO_2 has been shown to be the result of increased Ce^{3+} ions and oxygen vacancies produced as a result of size reduction. Interestingly, the lattice strain shown in Fig. 3(c) decreases with increasing Ni concentration for $x \leqslant 0.04$; however, above this concentration, an opposite behavior is observed. In many TM-doped oxide semiconductor systems, the dopants substitutionally occupy host sites at lower concentrations, and above a certain limit, additional interstitial incorporation of the dopant ions occurs.[6,21] We believe that the observed drastic change in η for $x>0.04$ is due to additional interstitial incorporation of Ni ions in the CeO_2 host lattice.

B. Transmission electron microscopy studies

HRTEM images (Fig. 4) display well defined lattice fringes indicating the crystallinity of the nanoparticles. The TEM estimates of the average particle size of the samples are also shown in Fig. 3(b) and agree well with the XRD estimates. Analysis of the EDP patterns (see insets of Fig. 4) matches with the reference data for bulk ceria, and all diffraction rings are accounted for.

C. Optical spectroscopy studies

The optical data collected at room temperature showed major changes in the overall diffuse reflectance and the absorption edge with even a small amount of doping (Fig. 5).

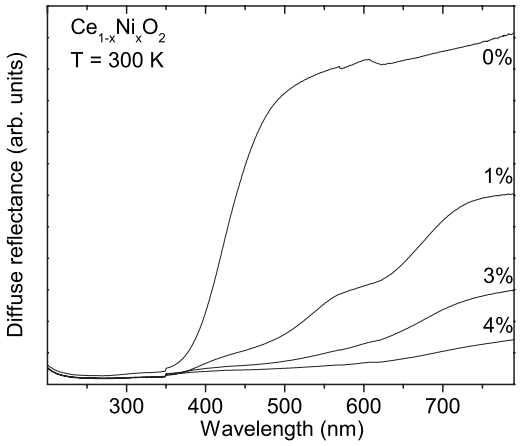

FIG. 5. Optical data from $Ce_{1-x}Ni_xO_2$ showing room temperature diffuse reflectance taken in the UV-visible range.

The significance of this is more visible after applying the Kubelka-Munk function,[21] given as $F(R)=(1-R)^2/2R$, where R is the magnitude of reflectance, to estimate the direct band gap energy [Fig. 3(c)]. The band gap energy E_g for $x=0$ of 3.80 eV is in close agreement with the direct band gap for pure ceria of 3.78 eV.[31] The band gap energy drops to 3.23 eV for $x=0.04$ and then rises up to 3.99 eV for $x=0.10$. The variation follows the strain data that were determined from analysis of the XRD patterns in a direct relationship [see Fig. 3(c)], indicating that the observed variation in E_g is related to the structural changes resulting from Ni incorporation. The variation in band gap for $x \leqslant 0.04$ is contrary to the reports of Zhang *et al.*[26] that smaller particle size causes an increase in the band gap energy of cerium oxide. However, the observed E_g variations with x in our $Ce_{1-x}Ni_xO_2$ samples are similar to that recently reported in $Sn_{1-x}Co_xO_2$,[21] in which a minimum in the band gap energy was observed at $x=0.01$. In $Sn_{1-x}Co_xO_2$, the observed changes for $x>0.01$ were attributed to the extensive structural changes caused due to interstitial Co incorporation. We believe that in the $Ce_{1-x}Ni_xO_2$ system also, for $x>0.04$, the band gap increases due to the combined effect of additional interstitial Ni incorporation and the nanoparticle size effect.[26]

D. X-ray photoelectron spectroscopy studies

Figure 6(a) shows the Ni $2p_{3/2}$ spectral region of a representative set of the $Ce_{1-x}Ni_xO_2$ samples as well as the physical mixture of NiO and CeO_2. The physical mixture exhibits visible features at 854, 855.7, and 861 eV clearly. The presence of the 855.7 eV feature, which has been commonly attributed to Ni^{3+} surface states in addition to the features due to core Ni^{2+}, agrees well with that reported for NiO.[35–37] The general features of the Ni $2p_{3/2}$ core region of the $Ce_{1-x}Ni_xO_2$ samples and the observed peak position of ~855.1 eV are clearly different from that of NiO. This further confirms that the Ni ions in the $Ce_{1-x}Ni_xO_2$ samples are not present as NiO and that the chemical environment of the incorporated Ni ions in the doped samples is different from that of the Ni ions in NiO. Representative XPS data of the

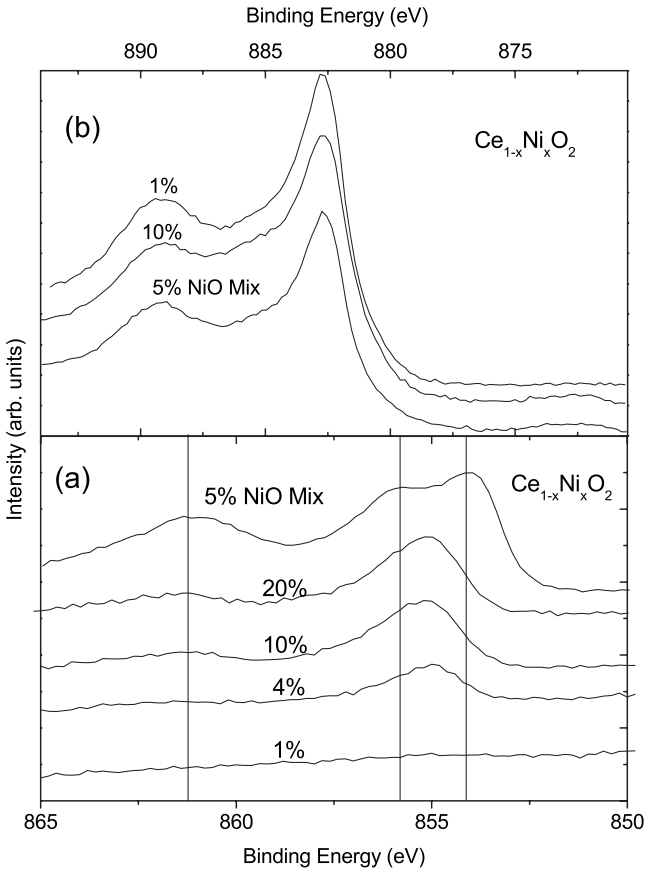

FIG. 6. (a) XPS of the Ni $2p_{3/2}$ region with lines through 854, 855.7, and 861 eV and (b) the Ce $3d$ region for selected samples.

Ce $3d_{5/2}$ core region of $Ce_{1-x}Ni_xO_2$ samples (with highest and lowest x) are shown in Fig. 6(b). In addition to the expected signature peaks of Ce^{4+}, weaker features corresponding to ~15% of the cerium ions in the Ce^{3+} state were also present. This is in agreement with similar reports on the presence of Ce^{3+} states in CeO_2 nanoparticles.[30]

E. Magnetic measurements

Hysteresis loops taken with a maximum field of ±10 kOe, shown in Fig. 7(a), display the FM properties of the $Ce_{1-x}Ni_xO_2$ samples. The magnetization M of the samples is weak and the loops had small coercivities in the range from 40 to 120 Oe. There is also a linear paramagnetic component χ_p for each sample, suggesting that not all of the dopant atoms participate in the FM ordering.[6] Figure 7(b) shows a plot of $M-\chi_pH$ displaying FM saturation, while Fig. 7(c) shows the low-field region of the as-collected data displaying the open hysteresis loops and illustrating the changes in coercivity and remanence. Both the saturation magnetizations M_s obtained from the $M-\chi_pH$ vs H data of Fig. 7(b) and remanent magnetizations M_r estimated from the as-collected M vs H data [Fig. 7(c)] show an increase as x increases to 0.04 and then a decrease for higher doping levels, as shown in Fig. 3(d). The observed changes in the magnetic properties with x mimic that observed in the lattice strain and band gap [Fig. 3(c)], suggesting that all of these characteristics are

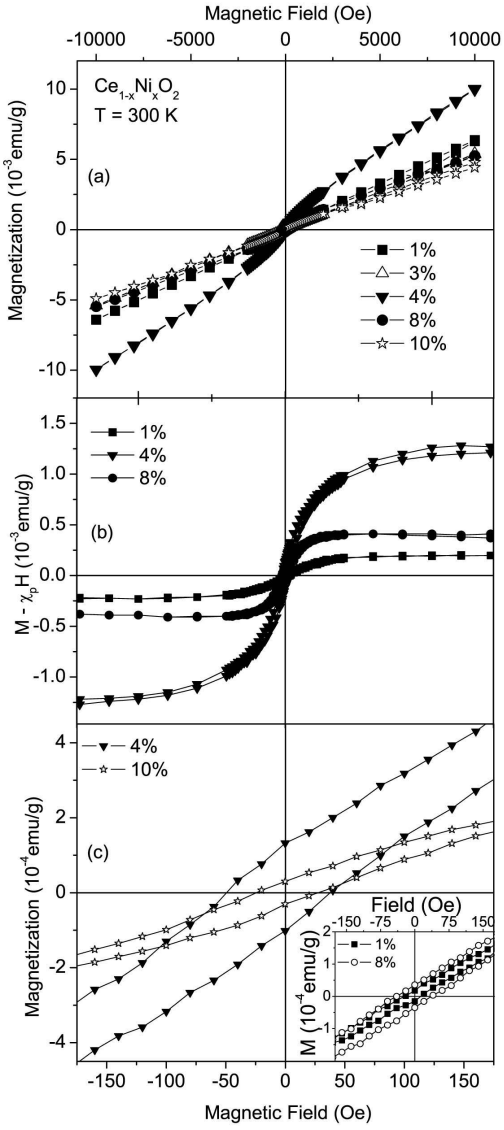

FIG. 7. Room temperature magnetic data showing (a) full M vs H hysteresis loops for all $Ce_{1-x}Ni_xO_2$ samples, (b) $M-\chi_pH$ vs H for $x=0.01$, 0.04, and 0.08, and (c) low-field region of the M vs H data showing the coercivity and remanence for $x=0.04$ and 0.10 with the inset showing the same for $x=0.01$ and 0.08.

related to the structural changes caused by the Ni ion incorporation in CeO_2. M vs H data collected for the physical mixture of NiO and CeO_2 (with $x=0.05$) is shown as Fig. 8, along with the M vs H data obtained from $Ce_{1-x}Ni_xO_2$ samples for $x=0$, 0.15, and 0.20. The absence of the saturating component in the magnetization data in the physical mixture helps rule out impurities as the cause of the observed FM behavior in samples with $0.01 \leqslant x \leqslant 0.10$. Since the physical mixture of NiO and CeO_2 does not show the FM behavior, observed magnetism in the doped samples therefore cannot be attributed to small amounts of NiO nanoparticle impurities formed during synthesis. The lack of a saturating component in the samples with $x=0$, 0.15, and 0.20 also rules out unknown impurities, since any such phases would result in spontaneous magnetization in all samples. Furthermore, the observed FM behavior and its dependence

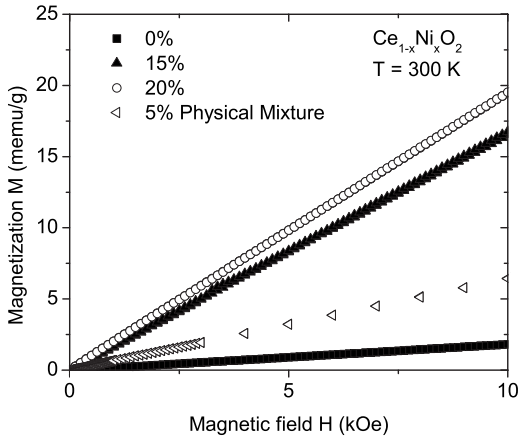

FIG. 8. Room-temperature M vs H data collected for $Ce_{1-x}Ni_xO_2$ for $x=0$, 0.15, and 0.20 and the same for the physical mixture containing 5% NiO in CeO_2.

on the Ni concentration are repeatable. The fact that these results are fully reproducible rules out the possible role of any random impurities.

Figure 9(a) displays high Curie temperatures (T_C) of 550 and 665 K for two of the $Ce_{1-x}Ni_xO_2$ samples with $x=0.04$ and 0.03, respectively. These T_C values are higher than the Néel temperature for nickel oxide ($T_N=523$ K) or the Curie temperature of metallic Ni (627 K) (Ref. 34) and once again illustrates that the observed magnetic behavior is not a result

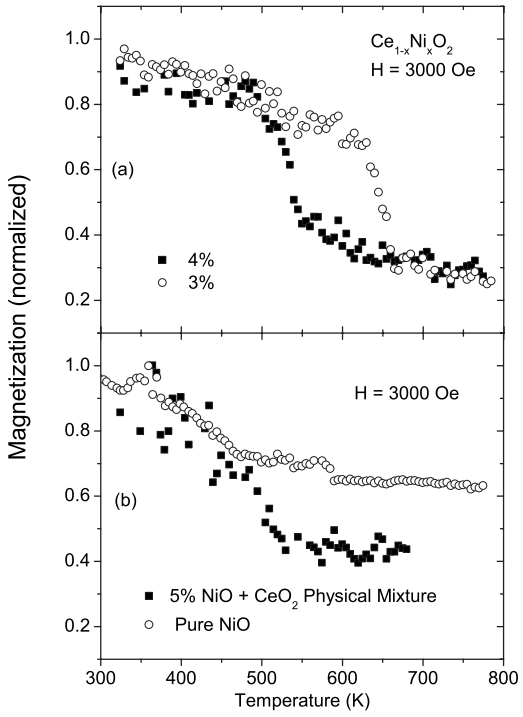

FIG. 9. (a) Plot of the normalized sample magnetization versus temperature showing the Curie temperature T_C for $x=0.03$ and 0.04, measured with an applied field of 3000 Oe. (b) Normalized M vs T data taken on pure NiO and the physical mixture of 5% NiO and CeO_2 with the same applied field for comparison.

of the formation of small amounts of nanoscale NiO or Ni particles, undetected in XRD. Figure 9(a) demonstrates that differing dopant concentrations result in a variation in the transition temperature, although the result may be somewhat unexpected since the data imply a lowering of T_C from 665 to 550 K when the dopant concentration increased from 3% to 4%. Based on reports[38–40] demonstrating similar irregular variation of T_C with x in GaMnAs, we attribute this result to differences in the defect concentrations,[38] grain size,[39] and/or domain structures[40] in the $Ce_{1-x}Ni_xO_2$ samples. Also shown [Fig. 9(b)] is the normalized M vs T data collected from the $x=0.05$ physical mixture of NiO and CeO_2 and the same for the pure NiO powder, displaying a much different behavior under these conditions than the doped samples. To the best of our knowledge, no FM Ni-Ce-O compound exists. Based on these reasons, we believe that the observed RTFM in $Ce_{1-x}Ni_xO_2$, albeit weak, is intrinsic.

F. Concluding remarks

Several recent studies[1,2,32,33] have indicated that oxygen vacancies, F centers, and defects in DMS systems play a major role in the magnetic exchange mechanism. In a recent paper, Coey *et al.*[2] proposed a model based on impurity-band exchange and density-functional calculations that ferromagnetism can be developed in oxides when the oxygen defect induced donor concentration δ is greater than the polaron percolation threshold δ_p and the cation concentration x is below the cation percolation limit x_p. For $x>x_p$, these studies have indicated antiferromagnetism or ferrimagnetism. Our results showing an increasing FM behavior for $x \leqslant 0.04$ and an opposite trend for higher x qualitatively agree with this picture. The substitutionally doped Ni^{2+} ions replacing Ce^{4+} or Ce^{3+} ions of the host lattice will produce oxygen vacancies for charge neutrality resulting in the FM interactions at lower concentrations ($x \leqslant 0.04$). In the F-center-mediated mechanism,[2] the radius of the electron orbital is a direct function of the dielectric constant. Since CeO_2 has a high dielectric constant of 26, the radius of the F-center electrons may be large enough to produce magnetic interactions at low Ni concentrations. As x increases (>0.04), a fraction of the Ni ions might enter into interstitial positions which require excess oxygen ions for charge neutrality. The higher concentration of the Ni ions and the lack of oxygen vacancies form an excellent recipe to produce antiferromagnetic interactions and to gradually destroy the FM behavior. However, more investigations to confirm the exact oxidation state of Ni ions and their host locations and to determine the role of oxygen stoichiometry are required to confirm these possibilities.

It is the authors' belief that the observed ferromagnetism is not a result of impurity phases for the following reasons: (i) Pure CeO_2 and heavily Ni doped samples do not show FM behavior, and this has been verified in several samples. If the FM was a result of a random impurity, then all samples would have clearly shown FM properties, which they do not. If the FM had been a result of Ni-based impurities, increasing the dopant concentration should have increased the strength of the observed FM, which again is not seen here.

Furthermore, with large amounts of Ni introduced into the system, the formation of Ni impurities should be visible in XRD; however, no unaccounted peaks appear in the diffraction data. (ii) The saturation magnetization increases and then decreases systematically with Ni doping, which would also not occur had the FM been caused by a random impurity. (iii) The lattice parameter changes indicate incorporation of Ni into the lattice, and the corresponding changes in the band gap energies and strain correlate well with the magnetization data. The observed variations are not likely to be due to an unknown impurity, since this would cause very random changes in data. (iv) The changes in Curie temperature with different dopant concentrations indicate that the resulting FM could not be from an unknown magnetic impurity, since this would result in the same Curie temperature observed for the different dopant concentrations used.

Thus, it has been shown that weak ferromagnetism can be produced at room temperature in sol-gel synthesized CeO_2 nanoparticles with nickel ion dopants. Ni doping has a strong influence on the microstructural, optical, and magnetic properties of CeO_2 nanoparticles. The magnetization of the material increases initially with increasing dopant concentration but drops considerably for levels above 4%. The sol-gel synthesis inherently removes the possibility of forming metallic nickel, and the experimental evidences rule out the presence of NiO, suggesting that the observed ferromagnetism is intrinsic.

ACKNOWLEDGMENTS

The research at Boise State University was supported in part by grants from the DOE-EPSCoR program (DE-FG02-04ER46142), Petroleum Research Fund (PRF No. 41870-AC10), NSF-Idaho-EPSCoR program (EPS-0447689), and NSF-CAREER (DMR-0449639) award. A portion of the research described in this paper was performed in the Environmental Molecular Sciences Laboratory, a national scientific user facility sponsored by the Department of Energy's Office of Biological and Environmental Research located at the Pacific Northwest National Laboratory.

*apunnoos@boisestate.edu

[1] A. H. MacDonald, P. Schiffer, and N. Samarth, Nat. Mater. **4**, 195 (2005).
[2] J. M. D. Coey, M. Venkatesan, and C. B. Fitzgerald, Nat. Mater. **4**, 173 (2005).
[3] S. A. Chambers and R. F. C. Farrow, Mater. Res. Bull. **28**, 729 (2003).
[4] J. Hays, A. Thurber, K. M. Reddy, A. Punnoose, and M. H. Engelhard, J. Appl. Phys. **99**, 08M123 (2006).
[5] P. V. Radovanovic and D. R. Gamelin, Phys. Rev. Lett. **91**, 157202 (2003).
[6] A. Punnoose, J. Hays, A. Thurber, M. H. Engelhard, R. K. Kukkadapu, C. Wang, V. Shutthanandan, and S. Thevuthasan, Phys. Rev. B **72**, 054402 (2005).
[7] S. B. Ogale *et al.*, Phys. Rev. Lett. **91**, 077205 (2003).
[8] T. Inoue, T. Ohsuna, L. Luo, X. D. Wu, C. J. Maggiore, Y. Yamamoto, Y. Sakurai, and J. H. Chang, Appl. Phys. Lett. **59**, 3604 (1991).
[9] Y. Nishikawa, T. Yamaguchi, M. Yoshiki, H. Satake, and N. Fukushima, Appl. Phys. Lett. **81**, 4386 (2002).
[10] Y. Nishikawa, N. Fukushima, N. Yasuda, K. Nakayama, and S. Ikegawa, Jpn. J. Appl. Phys., Part 1 **41**, 2480 (2002).
[11] J. Kang, X. Liu, G. Lian, Z. Zhang, G. Xiong, X. Guan, R. Han, and Y. Wang, Microelectron. Eng. **56**, 191 (2001).
[12] L. Tye, N. A. El-Masry, T. Chikyow, P. McLarty, and S. M. Bedair, Appl. Phys. Lett. **65**, 3081 (1994).
[13] A. S. Deshpande, N. Pinna, P. Beato, M. Antonietti, and M. Niederberger, Chem. Mater. **16**, 2599 (2004).
[14] V. Petrovsky, B. P. Gorman, H. U. Anderson, and T. Petrovsky, J. Appl. Phys. **90**, 2517 (2001).
[15] R. Ulrich, J. Vac. Sci. Technol. **11**, 156 (1974).
[16] R. Kersten, H. Mahlein, and W. Rauscher, Thin Solid Films **28**, 369 (1975).
[17] I. Kosacki, T. Suzuki, V. Petrovsky, and H. Anderson, Solid State Ionics **136-137**, 1225 (2000).
[18] Y. Chiang, E. Lavik, I. Kosacki, J. Lee, and H. Tuller, J. Am. Ceram. Soc. **79**, 1169 (1996).
[19] A. Punnoose, J. Hays, V. Gopal, and V. Shutthanandan, Appl. Phys. Lett. **85**, 1559 (2004).
[20] P. I. Archer, P. V. Radovanovic, S. M. Heaid, and D. R. Gamelin, J. Am. Chem. Soc. **127**, 14479 (2005).
[21] J. Hays, A. Punnoose, R. Baldner, M. H. Engelhard, J. Peloquin, and K. M. Reddy, Phys. Rev. B **72**, 075203 (2005).
[22] A. Punnoose, M. S. Seehra, W. K. Park, and J. S. Moodera, J. Appl. Phys. **93**, 7867 (2003).
[23] D. H. Kim, J. S. Chung, H. Tanaka, H. Y. Lee, T. Kawai, J. Y. Won, S. H. Park, and J. C. Lee, J. Appl. Phys. **93**, 6125 (2003).
[24] X.-D. Zhou and W. Hubner, Appl. Phys. Lett. **79**, 3512 (2001).
[25] S. Tsunekawa, K. Ishikawa, Z.-Q. Li, Y. Kawazoe, and A. Kasuya, Phys. Rev. Lett. **85**, 3440 (2000).
[26] F. Zhang, S.-W. Chan, J. E. Spanier, E. Apak, Q. Jin, R. D. Robinson, and I. P. Herman, Appl. Phys. Lett. **80**, 127 (2002).
[27] A. Tiwari, V. M. Bhosle, S. Ramachandran, N. Sudhakar, J. Narayan, S. Budak, and A. Gupta, Appl. Phys. Lett. **88**, 142511 (2006).
[28] J.-G. Li, T. Ikegami, Y. Wang, and T. Mori, J. Solid State Chem. **168**, 52 (2002).
[29] D. Shannon, Acta Crystallogr., Sect. A: Cryst. Phys., Diffr., Theor. Gen. Crystallogr. **A32**, 751 (1976).
[30] S. Deshpande, S. Patil, S. Kuchibhatla, and S. Seal, Appl. Phys. Lett. **87**, 133113 (2005).
[31] T. R. Griffiths, M. J. Davies, and H. V. Hubbard, J. Chem. Soc., Faraday Trans. 2 **72**, 765 (1976).
[32] N. H. Hong, J. Sakai, N. T. Huong, N. Poirot, and A. Ruyter, Phys. Rev. B **72**, 045336 (2005).
[33] J. Philip, A. Punnoose, B. I. Kim, K. M. Reddy, S. Layne, J. O. Holmes, B. Satpati, P. R. Leclair, T. S. Santos, and J. S. Moodera, Nat. Mater. **5**, 298 (2006).
[34] W. L. Roth, Phys. Rev. **110**, 1333 (1958).
[35] T. L. Barr, J. Phys. Chem. **82**, 16 (1978); **82**, 1801 (1978).

[36] St. Uhlenbrock, Ch. Scharfschwerdt, M. Neumann, G. Illing, and H.-J. Freund, J. Phys.: Condens. Matter **4**, 7973 (1992).
[37] J. van Elp, H. Eskes, P. Kuiper, and G. A. Sawatzky, Phys. Rev. B **45**, 1612 (1992).
[38] K. W. Edmonds, K. Y. Wang, R. P. Campion, A. C. Neumann, N. R. S. Farley, B. L. Gallagher, and C. T. Foxon, Appl. Phys. Lett. **81**, 4991 (2002).
[39] K. C. Ku *et al.*, Appl. Phys. Lett. **82**, 2302 (2003).
[40] I. Kuryliszyn-Kudelska *et al.*, J. Magn. Magn. Mater. **272-276**, E1575 (2004); I. Kuryliszyn *et al.*, J. Supercond. **16**, 63 (2003).